Constraining the subducting slab in the 2-D inversion of MT data in Southern Tohoku, NE Japan

Dieno Diba[1], Makoto Uyeshima[1], Masahiro Ichiki[2], Shin'ya Sakanaka[3], Makoto Tamura[4], Yiren Yuan[1,5], Marceau Gresse[1,6], Yusuke Yamaya[6], and Yoshiya Usui[1]

[1]Earthquake Research Institute, the University of Tokyo
[2]Graduate School of Science, Tohoku University
[3]Graduate School of International Research Sciences, Akita University
[4]Research Institute of Energy, Environment, and Geology, Hokkaido Research Organization
[5]Institute of Geophysics, China Earthquake Administration
[6]National Institute of Advanced Industrial Science and Technology

Background

Several previous studies have analyzed the influence of the subducting slab in 2-D MT inversion (e.g., Matsuno et al., 2010; Evans et al., 2014). Matsuno et al. (2010), who interpreted MT data in the Mariana subduction system, showed that MT generally has minor sensitivity to the subducting slab because it is resistive. According to them, the regularization constraint at the slab surface had to be relaxed to recover a resistive slab and a conductive zone above it. Otherwise, this conductivity contrast would be unclear. Evans et al. (2014) treated MT data in the Cascadia subduction zone. They first performed a typical unconstrained inversion (uniform initial model) and found a moderately resistive slab. Then, they re-started the inversion with a resistive slab in the initial model, but it is free to change during inversion. The resistive slab remains in the final model, but the other structures look similar to the unconstrained inversion result.

Our MT data is in the southern part of Tohoku, NE Japan. We aimed to image the fluid distribution related to the magmatism and seismicity in the area. MT data were acquired on three parallel NW-SE profile lines across the island arc. In the previous SGEPSS meeting (2022/11/03), we showed the result of 2-D interpretation for each profile line under unconstrained inversion. We found that the subducting Pacific slab is somewhat resistive, as in Evans et al. (2014). Thus, we wanted to constrain the slab during the inversion by imposing a high resistivity body and comparing the result with the unconstrained inversion.

2-D finite triangular element inversion code

To accurately constrained the subducting slab, we developed a 2-D finite element inversion code. Triangular element is chosen because it can accommodate irregular structures, such as topography, bathymetry, and in this case, the inclined subducting slab. Also, a triangular mesh can accommodate tiny elements surrounding the stations. We implement the node-based finite element formulation (Rylander et al., 2013).

Gauss-Newton algorithm is used for minimizing the objective function. The data-space formulation, as in Usui et al., 2017, is used because it is more efficient than the model-space formulation. The objective function consists of a data misfit term and a regularization term. Given a triangular cell in the mesh, the regularization penalized the difference between its conductivity value and the conductivity of surrounding cells sharing the same edge (Fig 1(a)). To construct the sensitivity matrix, we used the reciprocity method for efficiency (Rodi, 1976).

The code was initially written in MATLAB, but then, for speed, it was translated to Julia Programming Language. Fig 1(b) shows a performance comparison between MATLAB and Julia for identical inversions. Julia reaches the final model faster than MATLAB. The speedup is 1.8 times, and it may scale up with the size of the problem. In the first iteration, Julia was slower than MATLAB because Julia compiled the code in the first iteration.

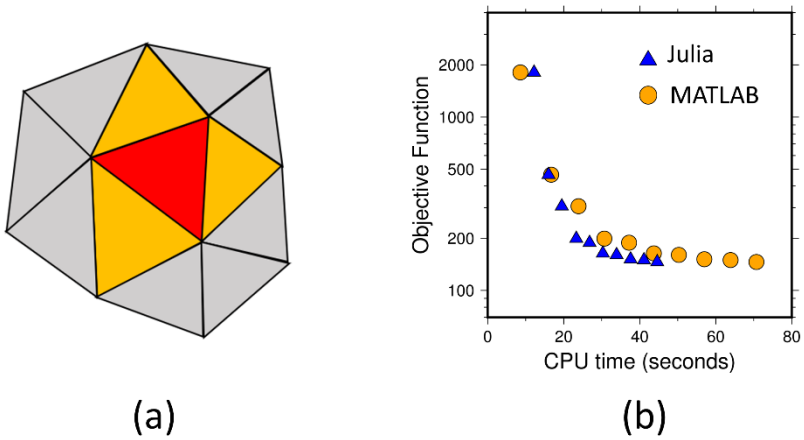

Figure 1. (a) Illustration of roughness penalty implemented in the newly developed inversion code. (b) Comparison of the performance between the code written in Julia and MATLAB given the same inversion problem. Here, Julia is faster than MATLAB.

Slab-constrained inversion results

With this inversion code, we investigated the influence of slab in our MT data. For each profile line, we performed inversions with different slab settings. We used 1k and 10k Ωm as testing resistivity

values of the slab. Also, in one experiment, the slab resistivity is fixed during inversion (referred to as slab-fixed inversion hereafter). In another experiment, the slab resistivity is free to change during inversion (referred to as slab-free inversion hereafter). The slab surface follows the trend of the hypocentres of inter-plate earthquakes. The thickness of the slab is 90 km, as in Ichiki et al. (2015).

Constrained inversion results show that the slab only affects the deeper structure greater than 80 km depth. The shallower structures are identical to those obtained by unconstrained inversion. It is reasonable because the slab is a deep structure, so it is effective for data at longer periods. In the slab-fixed inversion results, we found a conductive zone lying on the slab surface, commonly observed on the three profile lines. This conductive zone is less evident in unconstrained inversion, so this tendency is similar to Matsuno et al. (2010). The resistivity of this conductive zone is lower in the 10k Ωm inversion than in the 1k Ωm inversion. In slab-free inversions, the conductive zone is not detected as in unconstrained inversions. Also, the slab maintains its initial resistivity value, except in one line with a very strong conductor about 30 km above the slab. It is probably because of the screening effect of the conductor.

To investigate the conductive zone on the slab surface, we did a synthetic inversion test with hypothetically similar structures to that beneath our MT profile lines (Fig 2). In the true (or reference) model, a 10 Ωm conductor and a 1k Ωm subducting slab are embedded in a 100 Ωm Earth. The distribution of MT stations on the ground follows that of the actual MT stations. We calculated a synthetic dataset with periods similar to actual data and with added Gaussian noise of 2 %. As before, we performed slab-fixed and slab-free inversions with 1k and 10k Ωm slab resistivity.

The synthetic test result is shown in Fig 2. The conductor was well recovered regardless of the setting of inversion. But in contrast, the slab is poorly recovered in the unconstrained inversion result. Even in the slab-free inversion results, the slab does not remain clear due to the screening effect of the conductor. In the slab-fixed inversion results, the conductor elongates downward toward the slab surface, even in the 1k Ωm case (exact resistivity to the true model). This feature imitates that observed with actual MT data. Considering that the RMS of 1k Ωm slab-fixed inversion result is identical to the unconstrained inversion result, the elongation of the conductor might be an artifact of the inversion. Similarly, the conductive zone on the slab surface in the actual data inversion might also be an artifact and should be carefully considered.

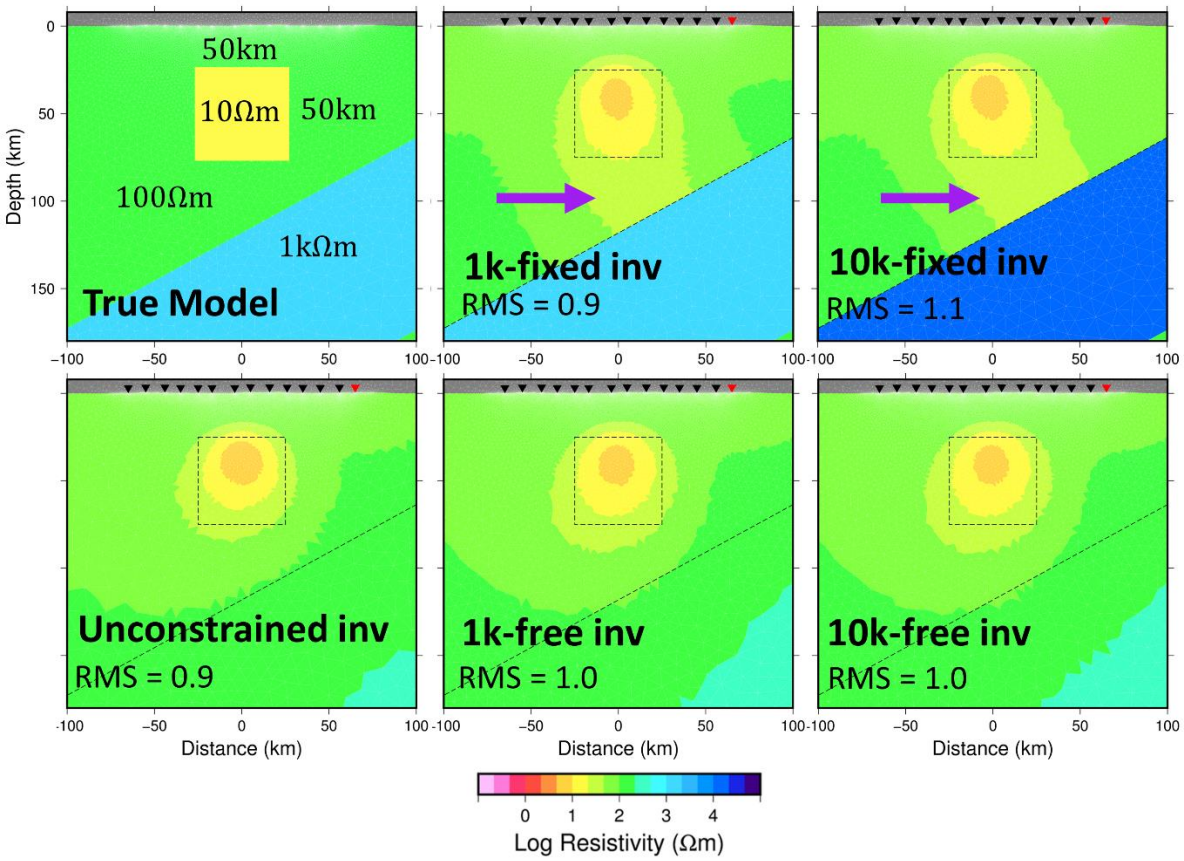

Figure 2. Synthetic test of a slab in the inversion at subduction zone margin. See text for details of slab-fixed and -free inversions. Purple arrows point to a conductive zone elongated from the central conductor to the subducting slab. Inverted triangles denote the MT stations, and the red ones denote the HMTF reference station.

Back to the actual MT data inversion, in terms of fitting, the results of slab-free and slab-fixed inversions generally have comparable data misfits to those of unconstrained inversion. It is also the case in Matsuno et al. (2010). In two of the three profile lines, constrained inversions yield a slightly smaller RMS than unconstrained inversions. However, according to a statistical F-test, this slight improvement is statistically insignificant. Therefore, for our MT data, we cannot say that including a slab in the inversion is necessary for a better fit.

For future work, we plan to interpret the data three-dimensionally. Perhaps, we will also perform a similar analysis of the slab in the inversion.

Reference

Evans RL, Wannamaker PE, McGary RS, Elsenbeck J (2014) Electrical structure of the central Cascadia subduction zone: The EMSLAB Lincoln Line revisited. Earth Planet Sci Lett 402:265-274

Ichiki M, Ogawa Y, Kaida T et al. (2015) Electrical image of subduction zone beneath northeastern Japan. J Geophys Res Solid Earth 120:7937-7965.

Matsuno T, Seama N, Evans RL et al. (2010) Upper mantle electrical resistivity structure beneath the central Mariana subduction system. Geochem Geophys Geosyst 11(9).

Rodi WL (1976) A technique for improving the accuracy of finite element solutions for magnetotelluric data. Geophys J R astr Soc 44:483-506.

Rylander T, Ingelstörm P, Bondeson A (2013). Computational electromagnetics 2nd Ed: Springer, New York.

Usui Y, Ogawa Y, Aizawa K et al. (2017) Three-dimensional resistivity structure of Asama Volcano revealed by data-space magnetotelluric inversion using unstructured tetrahedral elements. Geophys J Int 208:1359-1372.